DOI: 10.1002/ejic.200900922

Solid Solution $Sr_2Sc_{1+x}Re_{1-x}O_6$ with a Perovskite-Like Structure: Phase Transitions and Magnetic Properties

Daria Mikhailova,*[a,b] Narendirakumar Narayanan,[a,b] Andrea Voss,[b] Helmut Ehrenberg,[a,b] Dmytro M. Trots,[c,d] Clemens Ritter,[e] Jürgen Eckert,[b] and Hartmut Fuess[a]

Keywords: Phase transitions / Solid solutions / Perovskites / Magnetic properties / Neutron diffraction

The solid solution $Sr_2Sc_{1+x}Re_{1-x}O_6$ with a monoclinic perovskite-like structure has been prepared with the composition range $0 \le x \le 0.333$. When $x \le 0$, other phases compete with the formation of $Sr_2Sc_{1+x}Re_{1-x}O_6$. Crystallographic details of Sr_2ScReO_6 ($x = 0$) were investigated by neutron and synchrotron powder diffraction in the temperature range 10–1153 K. Upon cooling, Sr_2ScReO_6 undergoes structural phase transitions: from cubic $Fm\text{-}3m$ to tetragonal $I4/m$ at ca. 800 K and from tetragonal $I4/m$ to monoclinic $P2_1/n$ at ca. 350 K, and a two-phase field (monoclinic $P2_1/n$ + tetragonal $I4/m$) was observed below 75 K. The latter transition coincides with a magnetic rearrangement from the paramagnetic to antiferromagnetic state. Compositions with $x > 0$ demonstrate no antiferromagnetic ordering.

Introduction

Re-containing double perovskites A_2MReO_6, where A is an alkaline earth ion and M is Fe^{3+} or Cr^{3+}, have recently attracted great interest because of their large spin polarization and high Curie temperatures, T_c.[1–4] The cation size of the A ion has a significant influence on the structural, magnetic and magnetotransport properties of these compounds.[5–9] The most common distortion of the aristotype A_2MReO_6 structure (space group $Fm\text{-}3m$) is a tilting of the $(M,Re)O_6$ octahedral units, which leads to lower-symmetry hettotype structures and changing of T_c by the strengthening or weakening of a pdd–σ coupling.[6] For example, Ba_2FeReO_6 with a cubic symmetry shows metallic behaviour, a low Curie temperature and modest coercivity, while monoclinic Ca_2FeReO_6 is a semiconductor with a high Curie temperature and large coercivity.[5,6] The structure of Sr_2CrReO_6 is tetragonal below 260 K, the compound is metallic and has one of the highest known T_c values among the double perovskites (635 K), whereas Ba_2CrReO_6 is hexagonal and paramagnetic and Ca_2CrReO_6 is monoclinic, an insulator and has a low Curie temperature.[2,1] In these compounds, the Fe^{3+} ($S = 5/2$) or Cr^{3+} ($S = 3/2$) spins are tied ferromagnetically through coupling with itinerant electrons and magnetic moments on the Re site, and the conduction band is mainly composed of the 5d down-spin electrons of Re^{+5}. A second factor that can influence the magnetic properties of A_2MReO_6, such as saturation magnetization, is the M/Re cation disorder, or the mixed occupancy of one crystallographic site by both M and Re cations.[10] A lower degree of cation disorder results in higher values of magnetization.

Considerably less work has been done for compounds with a nonmagnetic M cation in A_2MReO_6 (M = Sc^{3+}, In^{3+}, Y^{3+} or Lu^{3+}). In this case, only Re^{+5} ($S = 1$) contributes to the magnetic properties. The Re sites in the structure form an *fcc* sublattice, and Re spins may be subject to geometrical frustration, which can cause complicated magnetic behaviour as proposed in the literature.[1] For example, Sr_2ScReO_6 is an insulator at room temperature and crystallizes in the monoclinic space group $P2_1/n$ with a 0% cation disorder. It undergoes an antiferromagnetic transition at $T_N = 75$ K and shows a pronounced hysteresis in susceptibility around T_N.[1] It has been suggested that the difference between heating and cooling is due to a first–order structural transition, which may be accompanied with magnetic ordering. However, this assumption has not yet been confirmed experimentally.

M_2MgReO_6 (M = Ca, Sr, Ba) with Re^{+6} (S = 1/2) are other examples in which "unusual" magnetism in complex Re oxides is observed:[11] significant hysteresis effects in magnetization were detected in these oxides at temperatures

[a] Institute for Materials Science, Darmstadt University for Technology,
Petersenstr. 23, 64287, Darmstadt, Germany
[b] Institute for Complex Materials, IFW Dresden,
Helmholtzstr. 20, 01069 Dresden, Germany
[c] Hamburger Synchrotronstrahlungslabor, DESY,
Notkestr. 85, 22607 Hamburg, Germany
[d] Bavarian Research Institute of Experimental Geochemistry and Geophysics,
University of Bayreuth,
Universitätsstr. 30, 95447, Bayreuth, Germany
[e] Institut Laue Langevin,
6, rue Jules Horowitz, Boîte Postale 156, 38042 Grenoble-Cedex 9, France
E-mail: d.mikhailova@ifw-dresden.de

up to 300 K, which reveal a ferromagnetic component in the magnetic structure and surprisingly high magnetic ordering temperatures. Detailed investigations of the crystal structure and the magnetic behaviour of Sr_2MgReO_6[12] and Sr_2CaReO_6[13] revealed a frustration-driven spin-glass state with a ferromagnetic component. On the contrary, Sr_2ZnReO_6[1] shows antiferromagnetism at room temperature and ferromagnetic ordering at low temperature. The crucial point in investigations of magnetism of Re-containing perovskites with Re as the only magnetic ion is the small magnetic moment of Re. In contrast to the expected $S = 1$ state of Re^{+5}, no direct determination of a magnetic structure by neutron diffraction was successful for such a system, which reflects the important role of spin–orbit coupling and structural antisite disorder on the resulting magnetic moment of Re.[14]

In this work we have investigated the phase stability of $Sr_2Sc_{1+x}Re_{1-x}O_6$ ($0 \leq x \leq 0.333$) as a function of x and the structural phase transformations in Sr_2ScReO_6 ($x = 0$) over a broad temperature range. Attempts were performed to elucidate the correlation between the underlying crystal structures and the resulting magnetic properties of the compounds. The obtained results will contribute to the experimental background for the discussion of "unconventional" magnetism in Re oxides with only Re as the magnetic ion.

Results and Discussion

Synthesis and Structural Characterization at Room Temperature

According to X-ray powder diffraction, the $Sr_2Sc_{1+x}Re_{1-x}O_6$ samples crystallize, at room temperature, with a monoclinic symmetry ($P2_1/n$) with the lattice parameters dependent on the cation composition, see Table 1. They represent a single phase for $0 < x \leq 0.333$. $Sr_7Re_4O_{19}$ or $Sr_{11}Re_4O_{24}$ and metallic Re were registered as additional phases for $x \leq 0$. Attempts to prepare the Re-deficient compound $Sr_2ScRe_{0.85}O_6$ with Re vacancies led to the appearance of $Sr_5Re_2O_{12}$ as a second phase. The single phase region corresponds to a formal oxidation state of Re between +5 and +6 in $Sr_2Sc_{1+x}Re_{1-x}O_6$. At a lower average Re oxidation state, other Re-containing phases compete with $Sr_2Sc_{1+x}Re_{1-x}O_6$ formation. The increasing Sc-content in the phase results in a higher degree of cation disorder and an increase in the unit cell volume, see Table 1. The values for the last compound shown are consistent with the larger cation size of Sc^{3+} (0.75 Å) relative that of Re^{5+} (0.58 Å).

For $x = 0$, an effect of the synthesis temperature on composition, structural and magnetic properties was studied for the samples prepared in the temperature range 1273–

Table 1. Phase compositions and structural parameters for $Sr_2Sc_{1+x}Re_{1-x}O_6$ samples.

Sample	$T_{synthesis}$ [K]	XRD Phase (w/w composition, %)	Lattice parameters a, b, c [Å] or β [°]	Cation disorder, n [%]	Volume [Å^3], w/w Re-content [%] {ICP-OES}
Kato et al.[1]	not reported	not reported	5.67502(3) 5.65283(3) 7.98686(3) 90.028(2)	0	256.218(4)
$Sr_2Sc_{0.67}Re_{1.33}O_6$	1273	$Sr_2Sc_{1+x}Re_{1-x}O_6$ (75) $Sr_7Re_4O_{19}$ (18) Re (7)	5.6553(2) 5.6522(2) 8.0168(2) 90.217(2)	5.8(2)	256.254(19)
Sr_2ScReO_6 (A)	1273	$Sr_2Sc_{1+x}Re_{1-x}O_6$ (88) $Sr_{11}Re_4O_{24}$ (10) Re (2)	5.6779(1) 5.6539(1) 7.9844(2) 90.04(1)	5.0(5)	256.312(10), 29.9(3)
Sr_2ScReO_6 (B)	1253	$Sr_2Sc_{1+x}Re_{1-x}O_6$ (89) $Sr_{11}Re_4O_{24}$ (9) Re (2)	5.6698(4) 5.6491(4) 7.9851(6) 90.05(3)	5.8(6)	255.745(33), 36.3(3)
Sr_2ScReO_6 (C)	1223	$Sr_2Sc_{1+x}Re_{1-x}O_6$ (99) Re (1)	5.6779(2) 5.6547(2) 7.9887(2) 90.03(2)	5.6(6)	256.492(24)
Sr_2ScReO_6 (D)	1173	$Sr_2Sc_{1+x}Re_{1-x}O_6$ (92) $Sr_{11}Re_4O_{24}$ (5) Re (3)	5.6889(2) 5.6687(2) 8.0072(3) 90.06(1)	6.8(1)	258.221(28), 35.0(3)
$Sr_2Sc_{1.15}Re_{0.85}O_6$	1273	$Sr_2Sc_{1+x}Re_{1-x}O_6$ (100)	5.6830(5) 5.6808(5) 8.0256(5) 90.05(1)	9.2(2)	259.099(38), 33.0(6)
$Sr_2Sc_{1.33}Re_{0.67}O_6$	1273	$Sr_2Sc_{1+x}Re_{1-x}O_6$ (100)	5.6969(8) 5.6810(7) 8.0120(6) 90.22(1)	18.2(2)	259.302(53), 26.5(7)

1173 K. It is known[15] that the formation of Re-containing complex oxides at high temperatures in sealed tubes can be accompanied by partial evaporation of rhenium and oxygen (mainly in form of Re_2O_7) in the reaction vessel, and therefore, a change in the initial Re and O stoichiometry in the sample. It can cause either Re and O deficiency in the solid phase, which results in different physical properties or the formation of other phases. According to ICP-OES measurements, while the Sr/Sc ratio in the samples with $x = 0$ corresponds to the "stoichiometric" ratio, the Re content after synthesis is lower than the "stoichiometric" Re content [37.1% (w/w)] and decreases with increasing synthesis temperature, see Table 1. The Re content for $x > 0$ is consistent with the stoichiometry [for example, 32.9% (w/w) for x = 0.15 and 27.3% (w/w) for x = 0.333]. According to the redox titration data, there is no oxygen deficiency in the phases for $x > 0$. The composition with $x = 0$ seems to correspond to the limits of the $Sr_2Sc_{1+x}Re_{1-x}O_6$ stability field, and, therefore, the phase composition and phase ratio are strongly dependent on external synthesis conditions such as temperature and the partial pressure of Re_2O_7.

Structural features that are dependent on the temperature were studied for $Sr_2Sc_{1+x}Re_{1-x}O_6$ with $x = 0$ (samples C and D from Table 1). The crystal structure of Sr_2ScReO_6 was first refined from X-ray powder diffraction at room temperature in the space group $P2_1/n$. The structure of Sr_2MnReO_6[16] has been chosen as an initial model for the refinement on the basis of the neutron and synchrotron experiments at room temperature because of their same space group and the very similar average ionic radii of Sc^{+3}+Re^{+5} and Mn^{+2}+Re^{+6}. The results obtained from the refinement of the neutron powder diffraction data are shown in Table 3. ScO_6 and ReO_6 octahedra in the structures are slightly distorted with average interatomic distances of 2.041 Å and 1.992 Å, respectively. Because of cation disorder in Sr_2ScReO_6, the average distance of Re–O is larger and that of Sc–O is smaller than the corresponding values in the completely ordered structure.[1]

Temperature-Induced Phase Transitions in Sr_2ScReO_6

Phase Transitions Above Room Temperature

According to the high-temperature synchrotron investigations, Sr_2ScReO_6 is cubic (*Fm*-3*m*) at 1073 K and shows two phase transitions when cooled down to room temperature: *Fm*-3*m* ↔ *I*4/*m* (to 800 K) and *I*4/*m* ↔ $P2_1/n$ (to 350 K). A transformation of some characteristic reflections, for example 400_c of the *Fm*-3*m* phase (visible already at 773 K) into two reflections 004_t and 220_t of the tetragonal *I*4/*m* phase (see patterns at 623 to 373 K) and into two reflections 220_m and 004_m of the monoclinic $P2_1/n$ phase (see pattern at 323 K), can be clearly seen in the range 2θ = 22.8–23.1° in sections of the synchrotron diffraction patterns (Figure 1). DSC measurements performed upon heating and cooling of the sample at a heating rate of 20 K/min have shown two small thermal effects at ca. 380 K and 790 K, which can be interpreted as the $P2_1/n$ ↔ *I*4/*m* and the *I*4/*m* ↔ *Fm*-3*m* phase transitions, respectively. The results of structure refinements are summarized in Table 2.

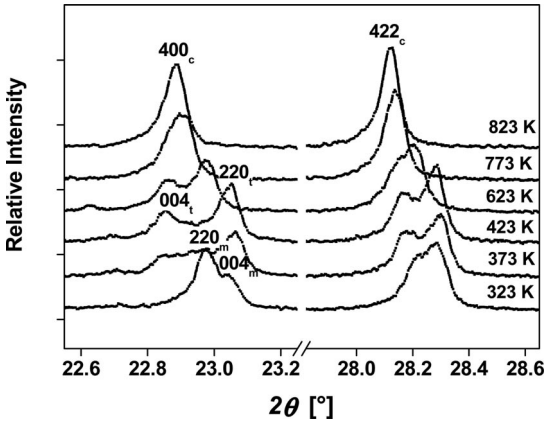

Figure 1. A section of the synchrotron powder diffraction patterns (λ = 0.79809 Å) of Sr_2ScReO_6, which demonstrate the cubic-to-tetragonal (723 K) and tetragonal-to-monoclinic (373 K) structural phase transitions in Sr_2ScReO_6. 400 and 422 reflections at 823 K belong to the cubic modification *Fm*-3*m*.

Table 2. Structural parameters for the high-temperature tetragonal and cubic modifications of Sr_2ScReO_6 at 623 K and 1023 K obtained from synchrotron diffraction. The cation disorder n was refined for both modifications, but changes only slightly within estimated standard deviations. The relevant interatomic distances (in Å) are also presented.

Temperature [K]	623	1023
Space group	*I*4/*m*	*Fm*-3*m*
a [Å]	5.66822(5)	8.06204(4)
c [Å]	8.05498(10)	–
V [Å^3]	258.796(5)	524.838(5)
Z	2	4
Sr	4d	8c
x	0	0.25
y	0.5	0.25
z	0.25	0.25
B [Å^2]	0.61(4)	1.76(4)
n [%]	10(1)	11(1)
Sc(1)	2b (0, 0, 0)	4b (0, 0, 0)
B [Å^2]	0.19(2)	0.33(2)
Re(1)	2a (0, 0, 0.5)	4a (0, 0, 0.5)
B [Å^2]	0.19(2)	0.33(2)
O(1)	4e	24e
x	0	0
y	0	0
z	0.254(2)	0.25
B [Å^2]	0.20(3)	0.25(4)
O(2)	8h	–
x	0.211(2)	–
y	0.688(2)	–
z	0	–
B [Å^2]	0.19(2)	–
O(3)	4e	–
Sc(Re)–O	1.954(1) (×4)	2.01550(4) (×6)
Sc(Re)–O	1.984(2) (×2)	2.01550(4) (×6)
Re(Sc)–O	2.135(1) (×4)	2.01550(4) (×6)
Re(Sc)–O	2.044(2) (×2)	2.01550(4) (×6)

The changes in the cell parameters and cell volume with temperature are displayed in Figure 2a and b for the three modifications of Sr_2ScReO_6.

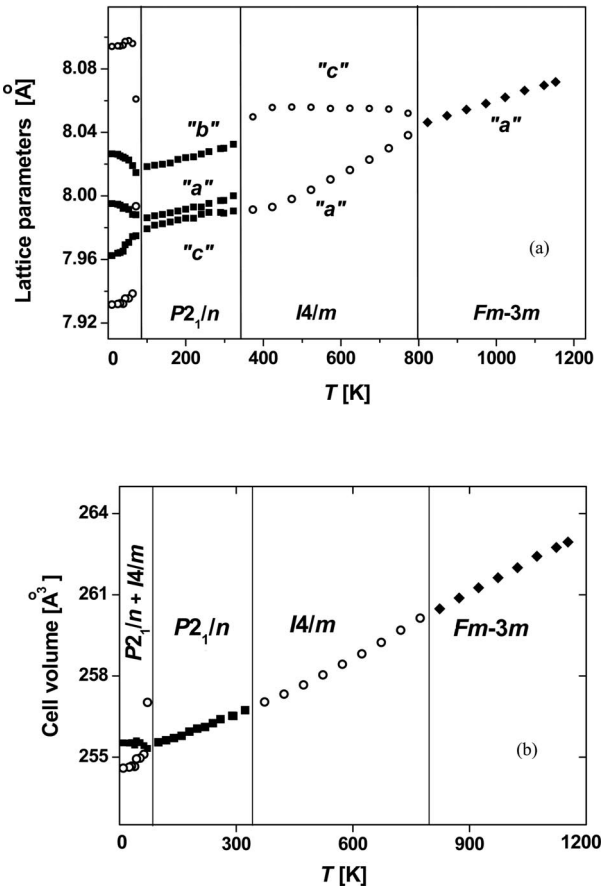

Figure 2. Temperature dependence of the (a) lattice parameters and (b) unit cell volume expansion of Sr_2ScReO_6 from synchrotron and neutron diffraction data. Estimated standard deviations obtained from Rietveld refinements are smaller than the size of the symbols. Parameters *a* and *b* of the monoclinic and tetragonal phases are multiplied in (a) by $\sqrt{2}$ for better comparison. The volumes in (b) are normalized to $Z = 2$, so that $V/2$ is plotted for space group *Fm*-3*m*. The data point at 72 K indicates an anomalous expansion of the tetragonal phase, which results in the transformation into the monoclinic form at about 75 K.

Both transformations in Sr_2ScReO_6 above room temperature represent displacive phase transitions, according to the classical Buerger's definition.[17] The transition *Fm*-3*m* ↔ *I*4/*m* is a second-order transition, as a result of the following criteria: (1) The space-group symmetry of the lower-temperature phase is a subgroup of the one of the higher-temperature phases; (2) ordering parameters such as the unit cell volume and the average Re–Re distance are continuous functions of temperature, see Figures 2 and 3. The transition *I*4/*m* ↔ $P2_1/n$ is from a thermodynamical point-of-view a first-order transition, because the space groups of the two coexisting phases do not obey a group–subgroup relationship.[18] The *I*4/*m* ↔ $P2_1/n$ transition is accompanied by a significant change in the lattice parameters (Figure 2a).

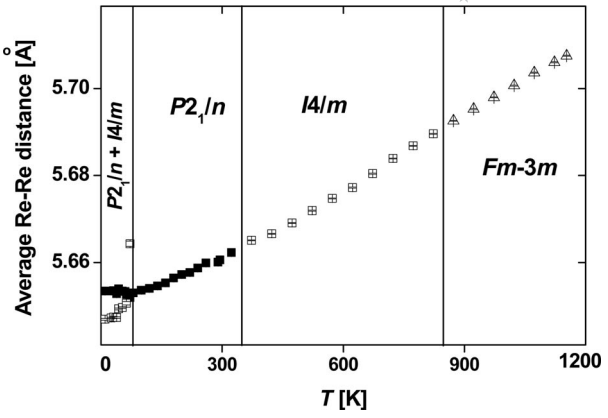

Figure 3. Temperature dependence of the average Re–Re distance (in Å) for all four Sr_2ScReO_6 polymorphs.

Phase Transition Below Room Temperature

A linear decrease in the lattice parameters with decreasing temperature was observed for monoclinic Sr_2ScReO_6 by both synchrotron and neutron powder diffraction from room temperature down to 80 K. Figure 4a and b represents relative changes in the cell parameters for the monoclinic modification, normalized to the values at 292 K. Below 80 K, a broadening of some reflections was detected by synchrotron diffraction and a splitting of the peaks could be resolved by neutron diffraction at a longer wavelength (Figure 5). No magnetic reflections in the low-temperature patterns were observed.

A clear peak splitting has also been observed by neutron scattering for monoclinic Ca_2FeReO_6.[5,19] It was attributed to the phase separation into two[5] or three[19] monoclinic phases below the magnetic-ordering temperature with identical or slightly different cell volumes, different magnetic structures and different coercivity according to the field dependence of the susceptibility. Our attempts to apply two crystallographic phases with the $P2_1/n$ symmetry but with different cell parameters (high-temperature monoclinic phase, HTMP and low-temperature monoclinic phase, LTMP) below 72 K analogously to the Ca_2FeReO_6 system gave a satisfactory refinement (Figure 6a). A small contribution from metallic Re [$P6_3/mmc$, 2.6% (w/w)] was also included as a third phase. Parameters *a* and *b* of the LTMP are very similar and are significantly shorter than those of HTMP, whereas the *c* parameter is longer, for example at 10 K $a = 5.6746(5)$ Å, $b = 5.6535(5)$ Å, $c = 7.9610(6)$ Å, $\beta = 90.186(8)°$ (HTMP) and $a = 5.6067(9)$ Å, $b = 5.6090(7)$ Å, $c = 8.0939(5)$ Å, $\beta = 90.01(3)°$ (LTMP). By using this refinement model, HTMP demonstrates a negative thermal expansion along the *a* and *b* axis and an increasing monoclinic angle β below 72 K, whereas LTMP shows a positive thermal expansion along the *a*, *b* and *c* axis down to 10 K. At 72 K, a difference between the *a* and *b* parameters for both HTMP and LTMP is not pronounced but that between the *c* parameters is. Because of the similarity of the *a* and *b* values of LTMP and the abrupt change in *a*, *b* and *c* relative to the HTMP, a discontinuous character of the

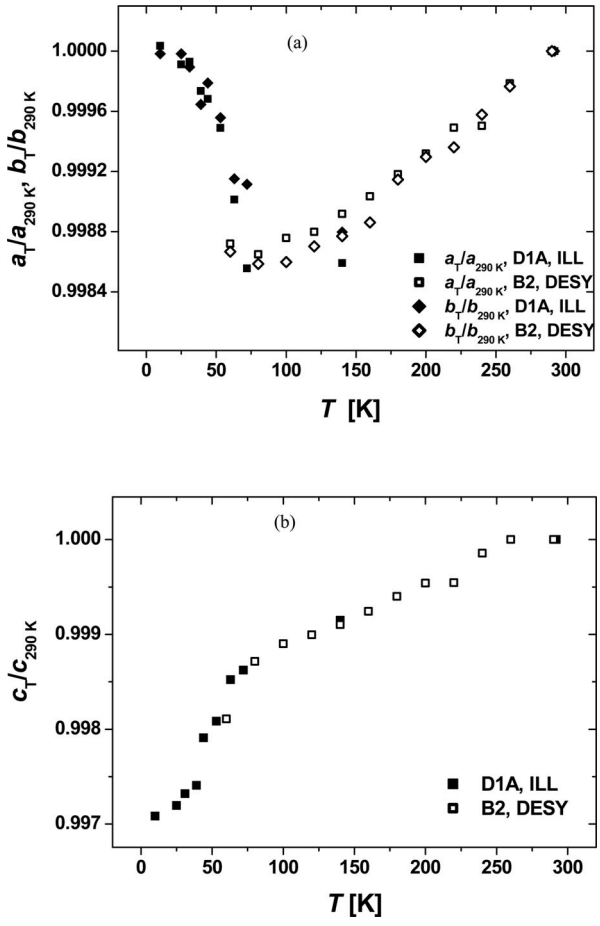

Figure 4. Relative changes of lattice parameters (a) *a* and *b* and (b) *c* for the monoclinic modification of Sr_2ScReO_6, normalized to the values at 290 K. Estimated standard deviations obtained from Rietveld refinements are smaller than the symbol sizes.

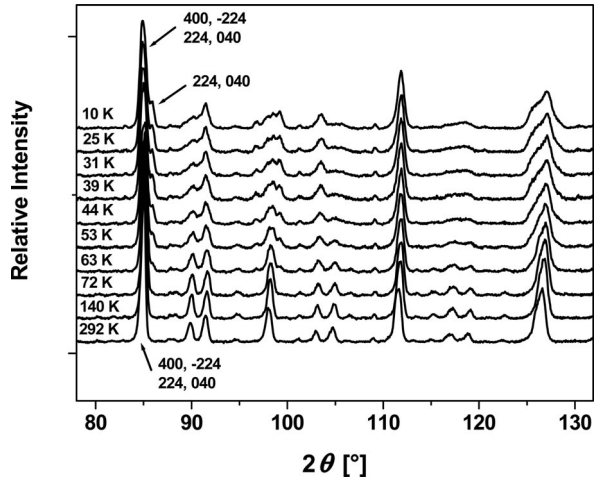

Figure 5. A section of neutron powder diffraction patterns (λ = 1.9090 Å) of Sr_2ScReO_6. A broadening of the reflections is observed below 72 K, which indicates a phase separation in the sample. On the basis of the coexistence of monoclinic and tetragonal modifications, the broadening of the reflection, for example at 2θ ca. 84°, can be explained as an overlap of four reflections 400, –224, 224, 040 at 292 K for the monoclinic modification. At 10 K, it corresponds to the presence of six reflections: 400, –224, 224, 040 for the monoclinic phase and 224, 040 for the tetragonal phase.

low-temperature phase transition and a tetragonal symmetry of the second phase at low-temperatures could be proposed.

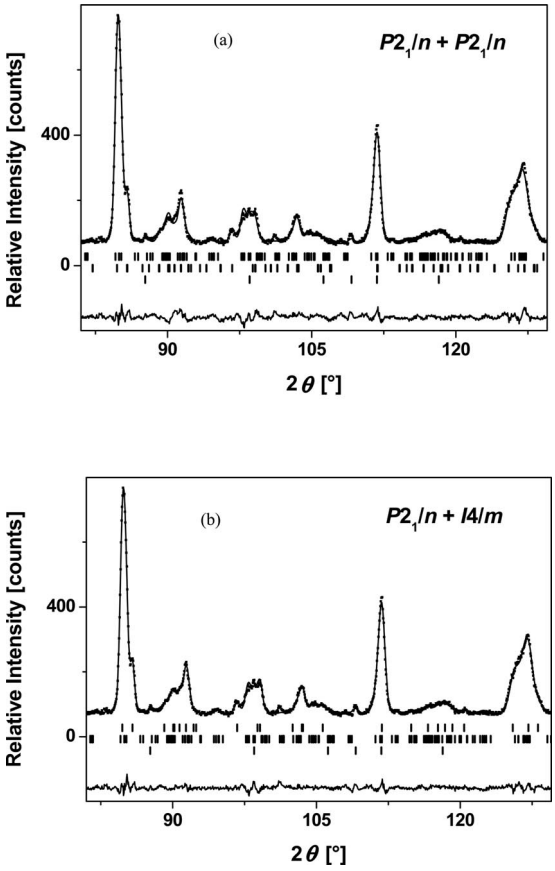

Figure 6. A part of the neutron powder diffraction pattern of Sr_2ScReO_6 at 10 K. For data refinement, (a) two monoclinic modifications with different lattice parameters or (b) the monoclinic and the tetrganonal modifications were used as a structural model. The third phase in both refinements is metallic Re (2.6%, w/w).

The best fit of the neutron data in the two-phase range can be reached, on the basis of a model similar to $Sr_2Fe_{0.75}Sc_{0.25}MoO_6$,[20] with two coexisting phases with $P2_1/n$ and $I4/m$ symmetry, see Figure 6b and Table 3. This indicates the re-entrant character of the tetragonal polymorph: $I4/m \leftrightarrow P2_1/n$ (to 80 *K*) and $P2_1/n \leftrightarrow I4/m$ (to 350 *K*). A coexistence of the monoclinic and tetragonal form below 80 K can be explained by the first-order character of this transition. The amount of tetragonal modification increases slowly with decreasing temperature from 9% (w/w) at 72 K to 44% (w/w) at 10 K. As an example, the raw data and the fitted Rietveld profile at 292 K and 10 K are shown in Figure 7. A normal positive thermal expansion is observed for the tetragonal low-temperature form in contrast to the anomalous behaviour of the monoclinic form, which is probably metastable over this temperature range (Figure 4a and b). The cell volume, as well as the average Re–Re distance of the stable low-temperature tetragonal modification, is smaller than those of the mono-

clinic phase (Figures 2 and 3). The average Re–O distance is always longer for the monoclinic modification in the whole two-phase temperature range, whereas the average Sc–O distance is longer for the tetragonal modification. At 72 K, close to the transition temperature, the tetragonal cell volume exceeds the volume of the $P2_1/n$ phase (Figure 2), probably an indication for the onset of its instability against the monoclinic form.

An alternative interpretation, based on the coexistence of an $I4/m$ phase hidden underneath the $P21/n$ phase with nearly the same lattice parameters in the range of 75–370 K, but detected below 75 K because of the more pronounced difference in lattice parameters at these low temperatures, was not confirmed.

There are a number of examples for inorganic–organic layered halide perovskites showing a re-entrant phase transition with low- and high-temperature polymorphs crystallizing in the same space group and with an intermediate phase with another symmetry, for example $(C_3H_7NH_3)_2PbBr_4$.[21,22] For this compound, a re-entrant polymorph with a lower symmetry and an incommensurate structure exists between two isomorphic modifications, which are stable at higher and lower temperature. The re-entrant phenomenon was interpreted as a coupling of the incommensurate order parameter with the interlayer distance, which itself depends on temperature.[21] The high-temperature isosymmetric form is more disordered than the low-temperature form. A characteristic feature of a re-entrant phase transition is a discontinuous change in the structural parameters, which corresponds to the first-order character.

For Sr_2ScReO_6, two aspects must be taken into consideration: (1) the structural phase transition from $P2_1/n$ to $I4/m$ below 80 K is accompanied by a magnetic phase transition as reported by Kato et al.,[1] which reduces

Table 3. Structure parameters for the monoclinic and low-temperature tetragonal modification of Sr_2ScReO_6 (Sample C from Table 1) obtained at room temperature, 53 K and 10 K with the D1A diffractometer. The cation disorder n = 10% was determined by X-ray diffraction at room temperature for the monoclinic modification and fixed in the structure refinement from neutron powder diffraction data for both modifications. The relevant interatomic distances (in Å) and angles (in °) are also given.

Temperature [K]	292	53		10	
Space group	$P2_1/n$	$P2_1/n$	$I4/m$	$P2_1/n$	$I4/m$
a [Å]	5.6760(2)	5.6731(4)	5.6112(3)	5.6762(4)	5.6084(2)
b [Å]	5.6534(2)	5.6509(4)	5.6112(3)	5.6533(4)	5.6084(2)
c [Å]	7.9862(3)	7.9710(5)	8.0977(6)	7.9629(5)	8.0941(4)
β [°]	90.063(8)	90.103(10)	90	90.188(7)	90
V [Å^3]	256.27(2)	255.53(2)	254.96(3)	255.52(3)	254.59(2)
Z	2	2	2	2	2
Sr	4e	4e	4d	4e	4d
x	0.0012(11)	0.0027(13)	0	0.0059(15)	0
y	0.5044(19)	0.5118(14)	0.5	0.5159(13)	0.5
z	0.2460(23)	0.2523(24)	0.25	0.2488(20)	0.25
B [Å^2]	0.72(5)	0.27(4)	0.27(4)	0.12(4)	0.12(4)
Sc(1)	2a (0, 0, 0)	2a (0, 0, 0)	2a (0, 0, 0)	2a (0, 0, 0)	2a (0, 0, 0)
B [Å^2]	0.35(3)	0.15(3)	0.15(3)	0.02(2)	0.02(2)
Re(1)	2b (0, 0, 0.5)	2b (0, 0, 0.5)	2b (0, 0, 0.5)	2b (0, 0, 0.5)	2b (0, 0, 0.5)
B [Å^2]	0.35(3)	0.15(3)	0.15(3)	0.02(2)	0.02(2)
O(1)	4e	4e	4e	4e	4e
x	–0.0448(8)	–0.0505(11)	0	–0.0557(11)	0
y	–0.0029(23)	–0.0090(16)	0	–0.0053(19)	0
z	0.2540(19)	0.2568(19)	0.2654(16)	0.2582(17)	0.2580(12)
B [Å^2]	0.79(4)	0.39(4)	0.39(4)	0.25(4)	0.25(4)
O(2)	4e	4e	8h	4e	8h
x	0.2342(22)	0.2279(21)	0.2060(32)	0.2334(22)	0.2126(16)
y	0.2714(25)	0.2838(24)	0.2916(31)	0.2693(27)	0.2959(15)
z	0.0315(12)	0.0271(21)	0	0.0303(14)	0
B [Å^2]	0.79(4)	0.39(4)	0.39(4)	0.25(4)	0.25(4)
O(3)	4e	4e		4e	
x	0.2688(20)	0.2657(20)		0.2742(23)	
y	0.7631(23)	0.7649(20)		0.7751(26)	
z	0.0181(11)	0.0227(19)		0.0152(15)	
B [Å^2]	0.79(4)	0.39(4)		0.25(4)	
Sc(Re)–O	2.036(11) (×2)	2.018(11) (×2)	2.005(16) (×4)	2.013(14) (×2)	2.044(9) (×4)
Sc(Re)–O	2.043(15) (×2)	2.068(15) (×2)	2.149(13) (×2)	2.029(15) (×2)	2.088(10) (×2)
Sc(Re)–O	2.044(15) (×2)	2.072(11) (×2)		2.081(13) (×2)	
Re(Sc)–O	1.982(16) (×2)	1.960(15) (×2)	1.900(13) (×2)	1.950(13) (×2)	1.959(10) (×2)
Re(Sc)–O	1.988(11) (×2)	1.980(11) (×2)	2.021(17) (×4)	2.016(14) (×2)	1.977(9) (×4)
Re(Sc)–O	2.005(14) (×2)	2.009(11) (×2)		2.020(15) (×2)	
Re–O–Sc	163.4(7)	162.3(6)	160.5(9)	161.9(8)	161.1(5)
Re–O–Sc	165.5(9)	163.4(7)	180	164.0(7)	180
Re–O–Sc	169.0(6)	167.5(6)	180	166.9(8)	180
Bragg R-factor [%]	3.56	3.17	4.05	3.72	3.03
R_f-factor [%]	4.37	3.53	2.47	3.88	1.81

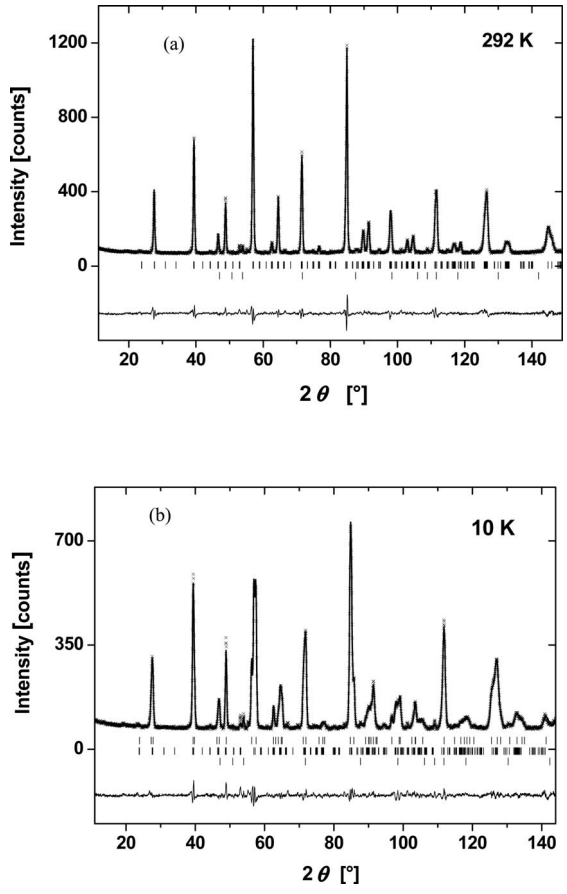

Figure 7. Neutron powder diffraction pattern of Sr_2ScReO_6 at (a) 292 K and (b)10 K. The solid lines indicate the calculated profiles for (a) monoclinic Sr_2ScReO_6 and hexagonal Re or (b) tetragonal and monoclinic Sr_2ScReO_6 and Re. Bragg peak positions for (a) monoclinic Sr_2ScReO_6 and Re, and (b) tetragonal and monoclinic Sr_2ScReO_6 and Re are marked in this sequence as tick marks.

the entropy of the low-temperature form of Sr_2ScReO_6; (2) cation ordering in the low-temperature tetragonal phase and monoclinic phase could be different. The refined cation ordering represents, in principle, the average value and does not include any inhomogeneity of the cation distribution in the sample. The low-temperature tetragonal modification could take place in domains with a higher degree of the cation ordering, which should support magnetic ordering. Although Bragg R- and R_f factors are somewhat smaller for the refinement with different values of cation ordering in both modifications, the strong correlation between cation ordering in the phase and thermal displacement parameters does not allow a conclusion on the different degrees of cation order in both modifications to be made.

The analysis of the structural details of the low- and high-temperature tetragonal modifications reveals a much stronger tetragonal distortion for the low-temperature form, which is stabilized by a magnetic interaction. Neutron powder diffraction does not allow to distinguish the type of antiferromagnetic ordering in Sr_2ScReO_6 because of the weak magnetic scattering of the low magnetic moments of the Re atoms, where the unusually large orbital moment of Re and spin–orbit coupling leads to very high transition temperatures.[2]

The crystal structures of the tetragonal and monoclinic modifications of Sr_2ScReO_6 at 10 K are compared in Figure 8. The discontinuous character of this first-order phase transformation is reflected in the temperature dependence of appropriate order parameters. Examples are the abrupt and simultaneous shifts of the Sr atoms from a general site 4e ($P2_1/n$) to the 4d site ($I4/m$) and of the O atoms from the general site 4e ($P2_1/n$) to the special positions on the 4e- and 8h sites ($I4/m$), accompanied by the transition from monoclinic to tetragonal symmetry. In the monoclinic modification with an $a^-a^-c^+$ octahedra tilt system according to Glazer's[23] notation, one O–O distance between neighbouring MO_6 octahedra is shorter (d_2, Figure 8b) and the other is longer (d_1, Figure 8b) relative to the corresponding O–O distance in the tetragonal phase with an $a^0a^0c^-$ octahedra tilting. Another ordering parameter is the oxygen displacement Δ (Figure 8a), which is non-zero in the tetragonal modification because of the alternating c^- rotations of the MO_6 octahedra about the [001] axis, but close to zero in the monoclinic form because of c^+ rotations. The temperature dependence of these order parameters is presented in Figure 9.

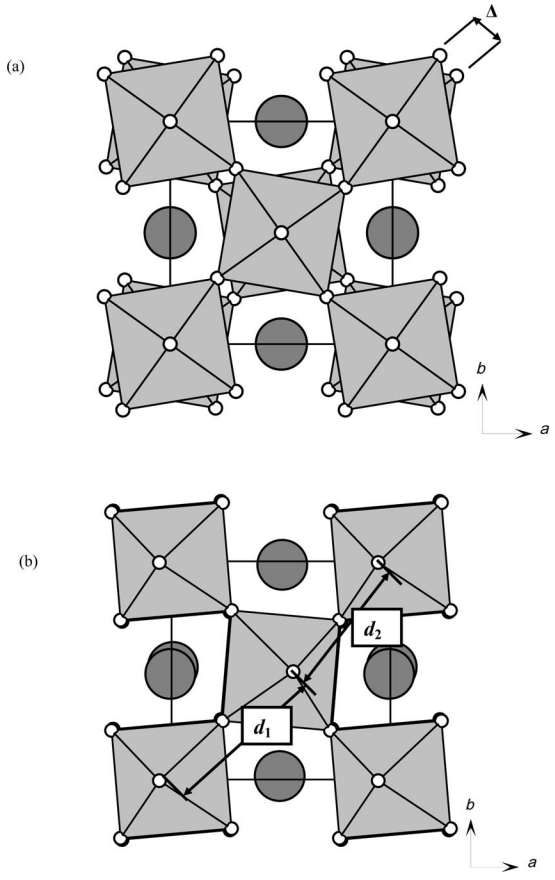

Figure 8. (a) Tetragonal body-centred ($I4/m$) and (b) monoclinic ($P2_1/n$) modifications of Sr_2ScReO_6 at 10 K along [001]. Small white spheres are O^{2-} ions, large dark grey spheres are Sr^{2+} and the octahedral faces belong to $[ScO_6]$ and $[ReO_6]$.

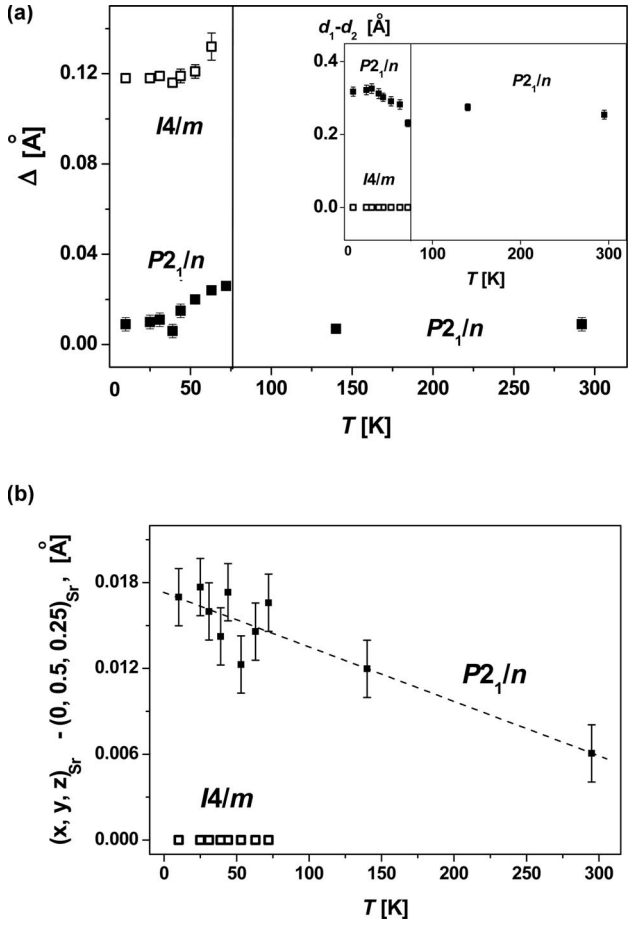

Figure 9. (a) Temperature dependence of the oxygen distances Δ (in Å) after projection of the $[ScO_6]$ and $[ReO_6]$ octahedra onto the *ab* plane, as shown in Figure 8a, for the tetragonal and monoclinic modifications of Sr_2ScReO_6 (neutron diffraction), together with temperature dependence of O–O distances d_1–d_2 (insert), see Figure 8b; (b) the shift of the Sr atoms to the 4e site in the monoclinic form from the 4d site in the tetragonal form.

Magnetic Properties of $Sr_2Sc_{1+x}Re_{1-x}O_6$

The temperature dependence of the magnetization was measured for $Sr_2Sc_{1+x}Re_{1-x}O_6$ ($0 \leq x \leq 0.33$) in both field-cooled (FC) and zero-field-cooled (ZFC) modes.

All Sr_2ScReO_6 samples ($x = 0$) show a maximum in magnetization below 70–75 K (Figure 10), in agreement with the report of Kato et al.[1] The maxima become more clearly visible in the temperature dependence of magnetization at higher fields (6 T). The Néel temperature of 75 K is again in good agreement with the observed structural transition between the high-temperature $P2_1/n$ phase and the low-temperature coexistence of the $P2_1/n$ and $I4/m$ phases. Most probably, the tetragonal body-centred phase is the phase with an antiferromagnetic ground state. Antiferromagnetic ordering reduces the entropy of the $I4/m$ phases as required from a thermodynamical point-of-view for a phase transformation during cooling. As the phase transition from $P2_1/n$ into $I4/m$ is a first order transition, a pronounced hysteresis in magnetization is observed as reported in the literature,[1] and successive experiments can give different magnetization values, because the phase ratio can also vary.

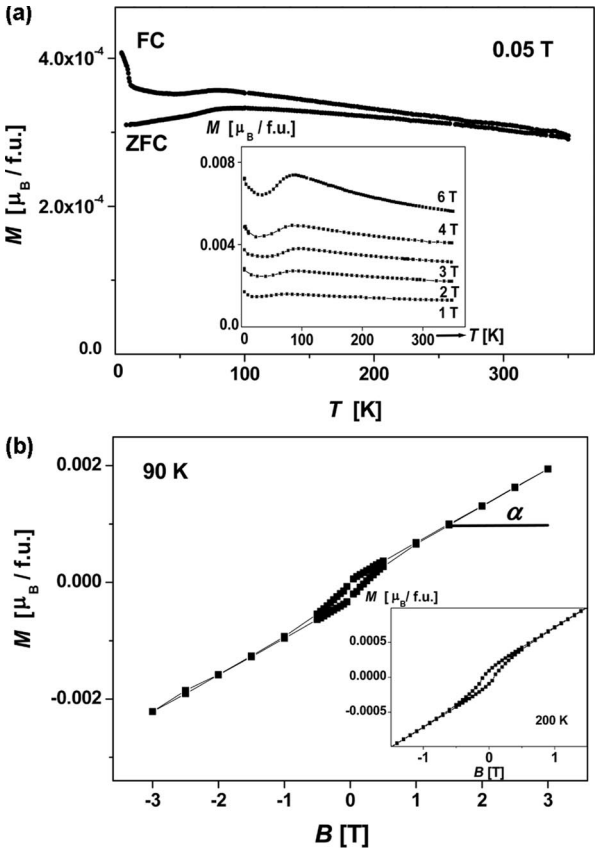

Figure 10. (a) Temperature dependence of magnetization and (b) magnetization hysteresis loops for Sr_2ScReO_6, prepared at 1273 K.

A difference between the FC and ZFC modes and a hysteresis loop in the field dependence of magnetization were observed for Sr_2ScReO_6, prepared at 1223 K and containing according to XRD only 1% (w/w) Re as second phase, up to 200 K (Figure 10). Other phases with Re in the Sr–Sc–Re–O system, such as $Sr_7Re_4O_{19}$,[24] $ScRe_2O_6$,[25] $Sr_{11}Re_4O_{24}$[26] or Sr_3ReO_6,[27] in small quantities (less than the detection limit of X-ray and neutron powder diffraction) could contribute to the observed magnetic behaviour. Only two oxides, $Sr_7Re_4O_{19}$[24] and $ScRe_2O_6$,[25] are known, which exhibit a ferromagnetic component above 100 K. Although the coercivity field strengths of 0.066 T at 10 K for $Sr_7Re_4O_{19}$ and 0.008 T at 10 K for $ScRe_2O_6$ are too weak relative to the observed value of 0.08 T for Sr_2ScReO_6 at 35 K (data not shown), and the shapes of the loops are different, the possible contribution of these phases cannot be excluded unambiguously. The rather high slope α in the high-field region indicates that the ferromagnetic component is only a small fraction of the total magnetic moment and that saturation has not been reached at ±6 T.

With increasing Sc content in $Sr_2Sc_{1+x}Re_{1-x}O_6$, a difference between the FC and ZFC data remains but the maximum in magnetization below 75 K disappears (Figure 11 inset). It is obvious that the magnetic interactions between

the Re moments depend strongly on the Re–Re distances and specific bond angles for the Re–O–Sc–O–Re pathways and are very sensitive to the cation disorder in the structure. It is known[2] and confirmed by calculations of total energies and densities of states (DOS) in the local spin-density approximation (LSDA) for ferromagnetic and antiferromagnetic spin configurations[28] that, for example, 100% cation order in double perovskites La_2MIrO_6 (M = Mn, Fe, Co) supports antiferromagnetic interaction, whereas ferromagnetism is predicted for a completely disordered phase. In the case of $Sr_2Sc_{1+x}Re_{1-x}O_6$, the increasing cation disorder from ca. 5% for $x = 0$ up to 18% for $x = 0.333$ leads probably to a suppression of the antiferromagnetic ordering. Although all samples with $x \geq 0$ demonstrate a divergence between the FC and ZFC data, which indicates the presence of a small ferromagnetic component, there is practically no hysteresis loop for $x > 0$ (data not shown).

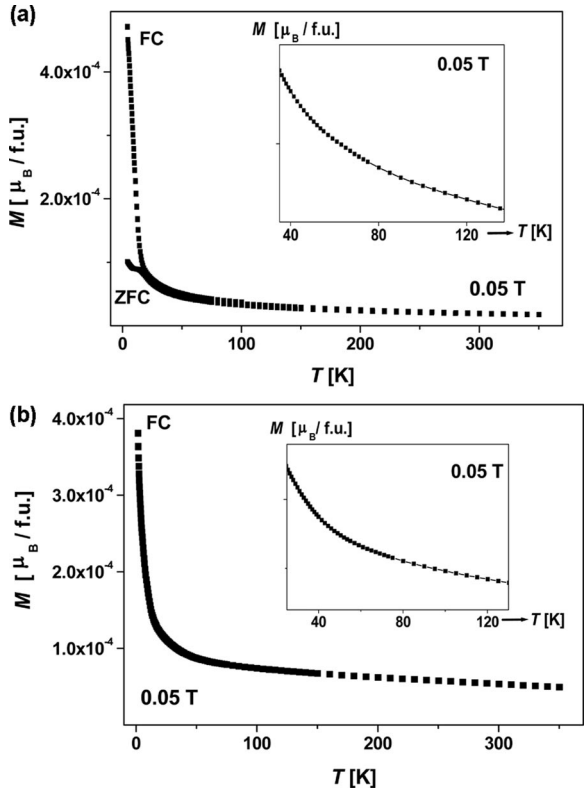

Figure 11. Temperature dependence of magnetization of (a) $Sr_2Sc_{1.15}Re_{0.85}O_6$ and (b) $Sr_2Sc_{1.333}Re_{0.667}O_6$ at 0.05 T.

In this context it is worth mentioning that two Sr_2ZnReO_6 modifications coexist at room temperature, monoclinic $P2_1/n$ and tetragonal $I4/m$. Magnetization measurements revealed a predominantly antiferromagnetic character for Sr_2ZnReO_6; however, the existence of a small hysteresis in the M(H) curves with a coercivity H_c of about 1.9 T at 20 K was detected as well, and related either to a spin canting of the Re^{+6} ions or a spin-glass like ground state as a result of geometrical frustrations.[1]

Conclusion

Sr_2ScReO_6 demonstrates three temperature-induced structural phase transformations, which are based on the tiltings of the MO_6 octahedra (M = Sc, Re) and a shift in the Sr positions. The low-temperature phase transition from $P2_1/n$ to $I4/m$ is accompanied by antiferromagnetic ordering, which might stabilize the higher symmetry of the low-temperature phase by the lower magnetic entropy. The magnetic behaviour of $Sr_2Sc_{1+x}Re_{1-x}O_6$ is rather complicated and depends strongly on the Re content: an increasing Sc content dilutes the Re sublattice, increases the average oxidation state of Re and the degree of cation disorder, which all suppress the antiferromagnetic ordering for $x \geq 0$. The presence of a ferromagnetic component in $Sr_2Sc_{1+x}Re_{1-x}O_6$ could be expected according to the second rule from Goodenough, Kanamori and Anderson:[29] an exchange interaction between a nonempty (Re^{5+}) and an empty orbital (Sc^{3+}) through a filled orbital (O^{2-}) favours a weak ferromagnetic order of the nonempty orbital as long as symmetry considerations allow such an exchange. Therefore, the magnetic interaction between the Re moments depend on the specific bond angles for the Re–O–Sc–O–Re pathways and on the Re–Re distances. The induced temperature-independent ferromagnetism seems to be an intrinsic behaviour of this complex perovskite system and does not seem to result from any undetected impurity. Further magnetic studies of other Sr_2MReO_6 double perovskites with nonmagnetic M^{3+} cations such as Ga or In, as well as magnetic investigations of single crystals of Sr_2ScReO_6, could further contribute to a more detailed understanding of "unconventional" Re^{5+} magnetism, which is characterized by rather strong couplings in comparison to the low magnetic moments.

Experimental Section

The syntheses of $Sr_2Sc_{1+x}Re_{1-x}O_6$ were performed in sealed silica tubes. The starting materials used were SrO, Sc_2O_3 (Strem Chemicals, 99.99%), Re (Alfa Aesar, 99.99%), Re_2O_7 (Alfa Aesar, 99.99%), ReO_3 (Strem Chemicals, 99.9%) and ReO_2 (Alfa Aesar, 99.99%). SrO was obtained by decomposition of $SrCO_3$ at 1323 K in a dynamic vacuum over 2 h. The starting components with a total mass of 1 g were weighed to an accuracy of 0.0005 g in a glove box, ground together in an agate mortar and pressed into pellets, which were then placed in a silica tube. The tube was evacuated and placed into a muffel furnace. The synthesis temperature was 1173–1273 K. After 30–33 h, the sealed tubes were quenched from 873 K in air.

Phase analysis and determination of cell parameters were carried out using X-ray powder diffraction (XPD) with a STOE STADI P diffractometer (Mo-$K_{\alpha 1}$ radiation, $\lambda = 0.7093$ Å) in transmission mode.

The low-temperature structure of Sr_2ScReO_6 was investigated both by synchrotron powder diffraction at HASYLAB/DESY (Hamburg, Germany) at beamline B2[30] and by neutron powder diffraction at the Institut Laue Langevin (Grenoble, France) on the powder diffractometer D1A. The high-temperature structures of

Sr_2ScReO_6 were studied with synchrotron diffraction at beamline B2.

The investigations with synchrotron radiation were performed in Debye–Scherrer mode by using the on-site readable image-plate detector OBI[31] and a He closed-cycle cryostat or a STOE furnace equipped with a EUROTHERM temperature controller and a capillary spinner. A 0.3-mm quartz capillary was filled with powdered Sr_2ScReO_6 in the glove box under Ar atmosphere, sealed and mounted inside the cryostat or the STOE furnace. The data were collected upon heating in steps of 0.004° over the 2θ range from 5 to 70° in temperature steps of 50 K with the wavelength of 0.7981(1) Å, based on the positions of 8 reflections from a LaB_6 reference material. After heating to 1150 K and cooling, the sample was analyzed again at room temperature.

Neutron diffraction patterns for Sr_2ScReO_6 in cylindrical vanadium cans with a 5 mm diameter were recorded between 10 and 292 K with a wavelength of 1.9090 Å.

All diffraction patterns were analyzed by full-profile Rietveld refinements, by using the software package WinPLOTR.[32] The structure model was refined with an isotropic approximation for the thermal displacement parameters of all atoms, which were constrained into three groups: one value for all oxygen atoms, one for Sr and one common one for Sc and Re atoms to reduce the degree of correlation between B-site disorder and thermal displacement parameters. The cation disorder can be described by a parameter n as a measure for the mixed occupation of Sc and Re on one specific site. The value of n corresponds to the relative amount of the minor element on these sites: $n = 0$ refers to complete order and $n = 0.5$ to 50% of Re on the Sc site and vice versa, i.e. a random distribution of Sc and Re on both sites. For Sc-rich compositions, cation disorder was defined to be 0, if only Sc atoms occupy the 2b sites.

DSC measurements of Sr_2ScReO_6 were performed in the temperature range 313–823 K upon heating and cooling of the sample at 20 K/min under an Ar atmosphere.

The magnetic properties of M_2ScReO_6 were studied with a superconducting quantum interference device (SQUID) from Quantum Design. Measurements were performed in field-cooled and zero-field-cooled mode in the temperature range 1.8–350 K and with external magnetic field strengths of up to 6 T.

Quantitative determination of Sr, Sc and Re contents in $Sr_2Sc_{1+x}Re_{1-x}O_6$ was carried out by ICP-OES method (IRIS Intrepid II XUV, Thermo Fisher) by using a mixture of HCl (37%, p.a. Fa. Merck) and HNO_3 (65%, p.a. Fa. Merck) to dissolve the samples. Three independent measurements on weighed portions of about 30 mg were performed for each composition. The oxygen content in the phase was calculated from the average oxidation state of Re, which was determined by back redox titration with potentiometric registration of the endpoint (DL70 ES, Mettler-Toledo). Samples were dissolved in an excess of $K_2Cr_2O_7$ solution (6 M H_2SO_4) with known concentration, and the excess of $K_2Cr_2O_7$ was titrated with a 0.1 M solution of Fe^{II}. The Re valence state was determined in the same way with ReO_3 (Strem Chemicals, 99.9%) powder as a reference material: the obtained results correspond to the composition $ReO_{2.995(9)}$ and confirm the appropriateness of this method.

Acknowledgments

This work was supported by the Bundesministerium für Bildung und Forschung (BMBF) (FKZ 05K57OD2 & 05KS7OD2). The authors are indebted to Birgit Bartusch (Institute for Complex Materials, IFW Dresden, Germany) for performing the DSC measurements.

[1] H. Kato, T. Okuda, Y. Okimoto, Y. Tomioka, K. Oikawa, T. Kamiyama, Y. Tokura, *Phys. Rev. B* **2004**, *69*, 184412.
[2] D. Serrate, J. M. De Teresa, M. R. Ibarra, *J. Phys. Condens. Matter* **2007**, *19*, 023201.
[3] M. Sikora, C. Kapusta, M. Borowiec, C. J. Oates, V. Prochazhka, D. Rybicki, D. Zajac, J. M. De Teresa, C. Marquina, M. R. Ibarra, *Appl. Phys. Lett.* **2006**, *89*, 062509.
[4] A. Winkler, N. Narayanan, D. Mikhailova, K. G. Bramnik, H. Ehrenberg, H. Fuess, G. Vaitheeswaran, V. Kanchana, F. Wilhelm, A. Rogalev, A. Kolchinskaya, L. Alff, *New J. Phys.* **2009**, *11*, 073047.
[5] W. Westerburg, O. Lang, C. Ritter, C. Felser, W. Tremel, G. Jakob, *Solid State Commun.* **2002**, *122*, 201–206.
[6] J. M. De Teresa, D. Serrate, J. Blasco, M. R. Ibarra, L. Morellon, *Phys. Rev. B* **2004**, *69*, 144401.
[7] E. K. Hemery, G. V. M. Williams, H. J. Trodahl, *Phys. B* **2007**, *390*, 175–178.
[8] P. Majewski, S. Geprägs, A. Boger, M. Opel, A. Erb, R. Gross, G. Vaitheeswaran, V. Kanchana, A. Delin, F. Wilhelm, A. Rogalev, L. Alff, *Phys. Rev. B* **2005**, *72*, 132402.
[9] J. B. Philipp, P. Majewski, L. Alff, A. Erb, R. Gross, T. Graf, M. S. Brand, J. Simon, T. Walther, W. Mader, D. Topwal, D. D. Sarma, *Phys. Rev. B* **2006**, *68*, 144431.
[10] L. Balcells, J. Navarro, M. Bibes, A. Roig, B. Martínez, J. Fontcuberta, *Appl. Phys. Lett.* **2001**, *78*, 781–783.
[11] K. G. Bramnik, H. Ehrenberg, J. K. Dehn, H. Fuess, *Solid State Sci.* **2003**, *5*, 235.
[12] C. R. Wiebe, J. E. Greedan, P. P. Kyriakou, G. M. Luke, J. S. Gardner, A. Fukaya, I. M. Gat-Malureanu, P. L. Russo, A. T. Savici, Y. J. Uemura, *Phys. Rev. B* **2003**, *68*, 134410
[13] C. R. Wiebe, J. E. Greedan, G. M. Luke, *Phys. Rev. B* **2002**, *65*, 144413.
[14] J. M. Michalik, J. M. De Teresa, C. Ritter, J. Blasco, D. Serrate, M. R. Ibarra, C. Kapusta, J. Freudenberger, N. Kozlova, *EPL* **2007**, *78*, 17006.
[15] D. Mikhailova, H. Ehrenberg, H. Fuess, *J. Solid State Chem.* **2006**, *179*, 3672–3680.
[16] G. Popov, M. V. Lobanov, E. V. Tsiper, M. Greenblatt, E. N. Caspi, A. Borissov, V. Kiryukhin, J. W. Lynn, *J. Phys. Condens. Matter* **2004**, *16*, 135–145.
[17] J. M. Buerger in "*Phase Transformation in Solids*" (Eds.: R. Smoluchowski, J. E. Mayer, W. A. Weyl), New York, Wiley, **1951**.
[18] C. J. Howard, B. J. Kennedy, P. M. Woodward, *Acta Crystallogr., Sect. B* **2003**, *59*, 463–471.
[19] E. Granado, Q. Huang, J. W. Lynn, J. Gopolakrishnan, R. L. Greene, K. Ramsha, *Phys. Rev. B* **2002**, *66*, 064409.
[20] C. Ritter, J. Blasco, J.-M. De Teresa, D. Serrate, L. Morellon, J. Garcia, M. R. Ibarra, *Solid State Sci.* **2004**, *6*, 419–431.
[21] Y. Abid, *J. Phys. Condens. Matter* **1994**, *6*, 6447–6454.
[22] W. Depmeier, *Z. Kristallogr.* **2009**, *224*, 287–294.
[23] A. M. Glazer, *Acta Crystallogr., Sect. Acta Crystallogr., Sect. B* **1972**, *28*, 3384–3392.
[24] K. G. Bramnik, H. Ehrenberg, H. Fuess, *J. Solid State Chem.* **2001**, *160*, 45–49.
[25] D. Mikhailova, H. Ehrenberg, G. Miehe, D. Trots, C. Hess, R. Schneider, H. Fuess, *J. Solid State Chem.* **2008**, *181*, 190–198.
[26] K. G. Bramnik, G. Miehe, H. Ehrenberg, H. Fuess, A. M. Abakumov, R. V. Shpanchenko, V. Yu. Pomjakushin, A. M. Balagurov, *J. Solid State Chem.* **2000**, *149*, 49–55.
[27] B. L. Chamberland, G. Levasseur, *Mater. Res. Bull.* **1979**, *14*, 401–407.
[28] M. Uhl, S. M. Matar, B. Sibechicot, *J. Magn. Magn. Mater.* **1998**, *187*, 201–209.
[29] P. W. Anderson in *Exchange in Insulators* (Eds.: G. Rado, H. Suhl), Academic Press, New York, **1963**.

[30] M. Knapp, C. Baehtz, H. Ehrenberg, H. Fuess, *J. Synchrotron Radiat.* **2004**, *11*, 328–334.
[31] M. Knapp, V. Joco, C. Baehtz, H. H. Brecht, A. Berghaeuser, H. Ehrenberg, H. von Seggern, H. Fuess, *Nucl. Instrum. Methods Phys. Res., Sect. A* **2004**, *521*, 565–570.
[32] T. Roisnel, J. Rodriguez-Carvajal, *Mater. Sci. Forum* **2001**, *378–381*, 118–123.

Received: September 16, 2009
Published Online: February 3, 2010

